# DC-Link Voltage Sensorless Control Technique for Single-phase Two-stage Photovoltaic Grid-connected System

N.E. Zakzouk [#1], A.K. Abdelsalam [#2], A.A. Helal[#3], and B.W. Williams [*4]

[#] *Electrical and Control Engineering Department*
*Arab Academy for Science, Technology and Maritime Transport*
*Alexandria, Egypt*
[1] nahlaezzeldin@hotmail.com
[2] kadry_2012@yahoo.com
[3] ahmedanas@aast.edu

[*] *Electronics and Electrical Engineering Department*
*Strathclyde University*
*Glasgow, United Kingdom*
[4] barry.williams@strath.ac.uk

***Abstract*— Control techniques, applied to single-phase two-stage grid-connected photovoltaic (PV) systems, mainly achieve functions of maximum power point tracking (MPPT), voltage adjustment at inverter DC-link, and grid current control. Conventional control techniques require measurements of PV voltage and current, DC-link voltage, and grid voltage and current. Commonly, sensorless techniques are proposed to simplify system implementation and decrease its entire size and cost. However, most focus on eliminating PV voltage and/or current sensors. In this paper, a sensorless technique is proposed which keeps PV sensors, but eliminates the expensive high DC-link voltage sensor by mitigating the inverter DC-link voltage control loop. Alternatively, voltage regulation at inverter DC-link is achieved through power balance guarantee at this link. Hence, control complexity is minimized and system stability is enhanced. Moreover, the entire system implementation is simplified and its dynamic response is improved during sudden irradiance changes. Simulation work is carried out to verify the effectiveness of the proposed technique when compared to the conventional one regarding their transient and steady-state performance under varying irradiance conditions.**

***Keywords:*** **photovoltaic source, utility interface, voltage source inverter, energy balance at inverter DC-link, DC voltage control loop, sensorless control technique.**

## I. INTRODUCTION

Among current renewable energy resources, photovoltaic (PV) energy has gained much interest as a noise and pollution free source. Furthermore, it has the ability to be expanded and utilized in arid areas [1]. Nowadays, common distributed energy resources (DERs), particularly PV sources, are increasingly being connected to utility for best utilization of their produced electric power [2]. For PV-grid interface, a number of methods are used, among which the string inverter technology is widely used at present [3]. In this method, a number of PV modules are connected in a series arrangement; called a string, and each string has its own inverter. Thus, the MPP of each PV string is separately optimized and the PV system can be expanded easily by adding additional strings with their relative inverters [4].

For low-power (< 10 kW) applications, DERs are usually connected to the AC grid through a single-phase voltage source inverter (VSI) at low voltage (110-220V) [5]. For successful PV string-grid interface, a number of requirements arise [6, 7]; maximum power point tracking (MPPT), voltage regulation at inverter DC-link, and grid current control. To achieve the latter, two topologies exist [3]; single-stage and two-stage topologies. The single-stage topology involves a single inverter stage to achieve all the previous tasks in order to reduce component count and increase conversion efficiency [8]. However, this inverter must be carefully designed to handle the double line frequency voltage ripples that appear at its DC-link due to single-phase connection [9]. Furthermore, large electrolytic capacitors must be connected to the PV string to limit these ripples propagation in the PV power, thus reducing inverter life-time [10]. Alternatively, two-stage topology is investigated in which a power decoupling DC-DC stage is added before the inverter stage [11]. This stage decouples the energy change between the PV string and the inverter DC-link which limits the voltage ripple impact on the PV source. Moreover, transformation of PV voltage level can be achieved using this additional stage thus expanding its operating range [3].

Conventionally, maximum power point tracking (MPPT) is achieved by the DC/DC converter stage while the second inverter stage inhibits two control loops to deliver power to the grid [12-14]. The first is an outer voltage control loop at the inverter DC-link and the second is an inner current control loop which forces the inverter to produce a sinusoidal grid current at low THD and almost unity power factor. Thus, the

978-1-4799-2449-3/14/$31.00 ©2014 IEEE

conventional control strategy for single-phase two-stage system requires measurement of PV voltage and current to detect PV power and achieve MPPT, DC-link voltage, and grid voltage and current. Sensorless control techniques have been proposed for this configuration to eliminate PV current and/or voltage sensors [15-18]. Most are based on an MPPT scheme presented in [19] which relies on the fact that as the DC-link voltage is kept constant by the controller action at steady-state, the PV power and the regenerative power to the grid side should be in balance. Consequently, the grid current's amplitude is proportional to PV generated power, eliminating the need to detect this power. Thus, varying the chopper duty cycle to maximize the line current amplitude will result in PV MPPT without the need of PV sensors. However, response deteriorates in comparison with that of the conventional method which directly detects PV power because the response of this sensorless MPPT operation directly depends on the response of the inverter voltage control loop and in turn its grid current control loop [20].

In this paper, a novel sensorless technique is proposed. It depends on the idea that if the PV maximum power is forced to flow to the grid then energy balance at inverter DC-link is satisfied by nature and the DC-link voltage will stabilize without the need of the inverter voltage control loop. Hence, the proposed scheme keeps PV sensors to directly measure the PV power, but eliminates the expensive high DC-link voltage sensor, thus reducing system size and cost. Furthermore, voltage controller removal simplifies the overall control scheme and improves the dynamic response during irradiance changes. Finally, the MPPT process is achieved independent of the inverter current loop. In order to validate the proposed idea, simulation work using MATLAB/Simulink is carried out and the proposed technique performance is compared with that of the conventional one under sudden irradiance changes.

## II. SYSTEM UNDER CONSIDERATION

The considered system is a 1.5 kW, 220 V, 50 Hz single-phase transformer-less two-stage grid–connected PV system as shown in Fig. 1. The PV source is a string consisting of ten KD135SX_UPU PV arrays connected in series. The first stage is a boost converter responsible for MPPT, PV voltage boosting, and decoupling between PV source and the DC-link. The second stage inhibits a current-controlled voltage source inverter (VSI) for grid interface.

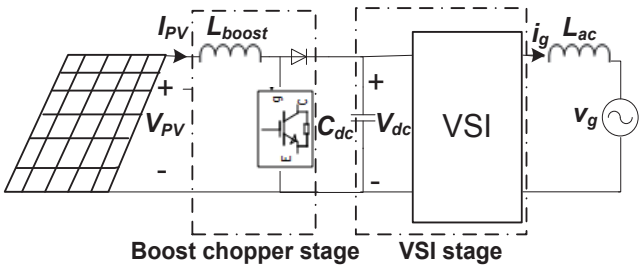


Fig. 1. PV-grid connected system under consideration

### A. Boost Converter

The gain of the boost converter, in the continuous power system, is given by [21];

$$G_{boost} = \frac{V_{o/p}}{V_{i/p}} = \frac{V_{dc}}{V_{PV}} = \frac{1}{1 - D_{boost}} \quad (1)$$

where $V_{pv}$ is the array voltage, $V_{dc}$ is the DC-link average voltage that should be chosen to provide proper modulation index of the inverter and $D_{boost}$ is the chopper duty ratio. The inductance of the boost converter ($L_{boost}$) is determined by selecting the acceptable current ripple passing through it ($\Delta I_L$) from (2):

$$\Delta I_L = \frac{D_{boost} V_{PV}}{f_{sw(b)} L_{boost}} = \frac{D_{boost}(1 - D_{boost}) V_{dc}}{f_{sw(b)} L_{boost}} \quad (2)$$

where $f_{sw(b)}$ is the switching frequency of the boost converter.

### B. Decoupling Capacitor at DC-Link

The DC-link capacitor ($C_{dc}$) is sized according to (3) to keep DC-link voltage fluctuations within specified limits [3];

$$C_{dc} = \frac{P_g}{\omega V_{dc} \Delta v_{dcp-p}} = \frac{P_g}{2\omega V_{dc} \Delta v_{dc}} \quad (3)$$

where $P_g$ is the average active power injected into the grid, $\omega$ is the line angular frequency in rad/sec, $\Delta v_{dcp-p}$ is the peak to peak DC-link voltage ripple and $\Delta v_{dc}$ is the amplitude of the DC-link voltage ripple.

### C. Voltage Source Inverter

The second stage involves a current controlled full-bridge VSI operating with sinusoidal pulse width modulation (SPWM) and a triangular carrier (15 kHz). The inverter output filter inductor ($L_{ac}$) is designed to mitigate the harmonics of the injected grid current. For high switching frequency and near unity power factor operation, the output voltage of the inverter is approximately equal to the utility voltage and the modulation index amplitude ($m_a$) is given by [22]

$$m_a = \frac{\hat{V}_g}{V_{dc}} \quad (4)$$

For single-phase inverters, $V_{dc}$ level is determined such that $m_a \leq 1$ so as to achieve acceptable total harmonic distortion in the grid current (*THDI*). Hence, $L_{ac}$ is calculated from (5) as follows [22];

$$\Delta I_g = \frac{V_{dc}}{2 f_{sw(i)} L_{ac}} \frac{1}{2\sqrt{3}} \sqrt{\frac{1}{2} m_a^2 - \frac{8}{3\pi} m_a^3 + \frac{3}{8} m_a^4} \quad (5)$$

where $f_{sw(i)}$ is the switching frequency of the inverter and $\Delta I_g$ is the rms ripple component of the grid current and can be calculated from (6) [22];

$$THDI = \frac{\Delta I_g}{I_{g(1)}} \times 100 \leq THD(required) \qquad (6)$$

where $I_{g(1)}$ is the root mean square (rms) value of the grid current fundamental component.

## III. POWER BALANCE AT DC-LINK

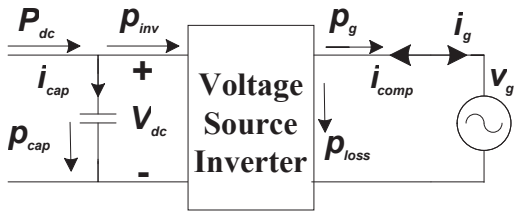


Fig. 2. Power flow at the DC and AC sides of the inverter

Assuming that the AC inductor is small and the AC line current ($i_g$) is sinusoidal and in phase with the AC grid voltage ($v_g$), equation (7) represents the power balance at the inverter DC-link [10, 12, and 23], as shown in Fig. 2.

$$P_{dc} = p_{inv} + p_{cap} \qquad (7)$$

where $P_{dc}$ is the input power to the DC-link, $p_{inv}$ is the instantaneous power supplied to the inverter, $p_{cap}$ is the instantaneous power in the DC capacitor ($C_{dc}$)

and $$p_{cap} = V_{dc} C_{dc} \frac{dv_{dc}}{dt} \qquad (8)$$

Hence, $$P_{dc} = p_{inv} + V_{dc} C_{dc} \frac{dv_{dc}}{dt} \qquad (9)$$

where $V_{dc}$, $v_{dc}$ are the average and the instantaneous values of the DC-link voltage respectively. Power at the inverter DC side ($p_{inv}$) will then flow through the inverter to the grid. However, inverter losses must be taken into account as shown in (10) otherwise a disturbance into the power balance equation will occur that results in a steady-state error in the DC-link voltage [23].

$$P_{dc} = p_g + p_{loss} + V_{dc} C_{dc} \frac{dv_{dc}}{dt} \qquad (10)$$

where, $p_g$ is the instantaneous active power injected to grid and $p_{loss}$ is the instantaneous inverter power loss.

To guarantee the previous power flow, the DC-link voltage is kept constant. Consequently, the term $\frac{dv_{dc}}{dt}$ tends to zero over one cycle and the DC-link power balance is satisfied. Hence, a control strategy is mandatory to achieve DC-link voltage regulation and grid interface.

## IV. PV-GRID INTERFACE CONTROL TECHNIQUES

PV-utility interface can be achieved, for the considered system, using conventional control technique [12-14]. However, a DC-link voltage sensorless technique is proposed to realize this interface. The control schemes of both techniques are analyzed, and then their performance is compared to validate the feasibility of the proposed one.

### A. Conventional Control Technique

The conventional control technique is shown in Fig. 3. Switching of the boost chopper is directly controlled using variable step incremental conductance MPPT algorithm [24]. On the other hand, DC-link voltage regulation and interface with utility are conventionally achieved by two control loops inhibited in the VSI; the outer DC-link voltage and the inner grid current control loops.

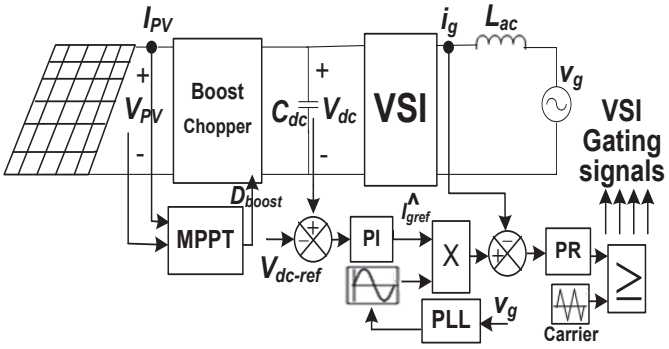


Fig. 3. Conventional control technique scheme

1) *Inner Grid Current Control Loop:* The inverter is required to inject a sinusoidal grid current with low THD and in phase with the grid voltage. Thus, the output of the DC-link voltage controller, which represents the reference grid current amplitude, is multiplied by a sinusoidal template obtained using a phase-locked loop (PLL) synchronized with the utility voltage. The current controller attempts to match the grid current with this reference sinusoidal current. The most common types of current controllers are: the proportional integral (PI) with feedforward controller and the proportional resonant (PR) controller. However, PR controllers have the ability to remove both the current's magnitude and phase steady-state errors without the need of voltage feedforward unlike the conventional PI controllers [6]. Thus a PR controller is considered with a transfer function given by;

$$G_{PR}(s) = K_P + K_I \frac{s}{s^2 + \omega^2} \qquad (13)$$

where *Kp* is the proportional gain, *Ki* is the resonant part gain and *w* is the resonant frequency of the controller which is the grid voltage angular frequency.

2) *Outer DC-link Voltage Control Loop:* This loop is responsible for DC-link voltage regulation by adjusting the amplitude of the sinusoidal reference grid current ($\widehat{I_{gref}}$). This current amplitude represents the active component of the reference grid current which indicates the instantaneous

amount of power available at the DC side of the inverter ($p_{inv}$) [23]. By accurate adjusting to this current amplitude and using a fast grid current controller of a bandwidth of a few kHz, power at the inverter side is transferred to the grid. Thus, power balance at the DC-link is achieved which makes $V_{dc}$ stabilizes at the required level.

However, in order to compensate for system losses shown in (10) (i.e. inverter losses and the energy required by $C_{dc}$ to keep $V_{dc}$ at a certain level), a decrease in the power available at the inverter side occurs which in turn decreases $\widehat{I_{gref}}$ . The latter imposes losses on the utility grid.

The DC-link voltage controller can be implemented as a simple proportional controller [13] or proportional integral (PI) one to minimize the DC-link voltage steady-state error [12]. The latter is applied and represented by the transfer function given in (14) where $K_p$ and $K_I$ are the applied controller's proportional and integral gains respectively,

$$G_{PI}(S) = K_P + \frac{K_I}{s} \tag{14}$$

However, the DC-link voltage controller must be precisely tuned to limit the oscillations reflected in the grid current reference. Otherwise, grid current THD can exceed the limit and a larger DC capacitor may be required, to overcome these oscillations, which in turn reduces the inverter life-time. Hence, this loop controller is designed for a low cross-over frequency (10-20 Hz) in order to attenuate the magnitude of the DC-link voltage ripple with double line frequency (100 Hz) [12].

### *B. Proposed DC-Link Voltage Sensorless Control Technique*

In this technique, MPPT is similarly achieved by sensing the PV voltage and current to be utilized by variable-step incremental conductance MPPT algorithm which directly controls the boost chopper switching. However, the proposed control technique involves only one control loop in the inverter stage which is the current control loop. Thus, the DC-link voltage control loop, with its PI controller, is eliminated. This simplifies the system control scheme, enhances its stability and improves its dynamic performance during irradiance changes. Moreover, the high DC-link voltage sensor is no longer required, reducing the system size and cost. The proposed sensorless control technique is shown in Fig. 4.

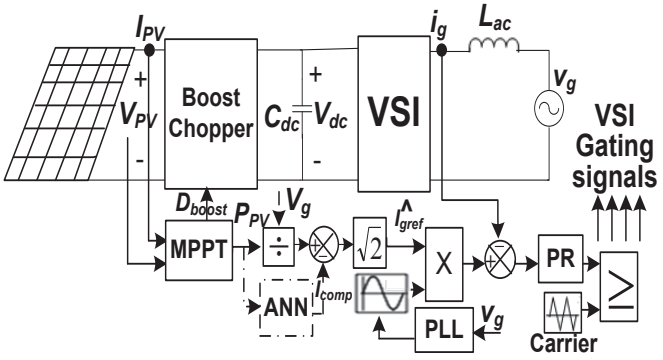


Fig. 4. Proposed sensorless control technique scheme

As previously explained, the reference grid current amplitude ($\widehat{I_{gref}}$) must be properly adjusted to transfer the inverter power to the grid. Thus, power balance at the DC link is achieved and $V_{dc}$ stabilizes at the required level. In the conventional technique, DC link voltage regulation and $\widehat{I_{gref}}$ adjustment are performed using the DC-link voltage control loop. Alternatively, this paper proposes a new method to stabilize the DC-link voltage and adjust $\widehat{I_{gref}}$ without the need of an outer voltage control loop. In the proposed control technique, the PV voltage and current are sensed to achieve MPPT and depending on the PV maximum power value, the amplitude of the reference grid current is adjusted. The grid current control loop forces the inverter to produce a sinusoidal current with a magnitude matching that of the reference current which corresponds to the tracked maximum PV power. Thus the PV maximum power is forced to flow to the inverter AC side satisfying the power balance at inverter DC-link which in turn forces the DC-link voltage to stabilize at a certain level without the need of a voltage controller

To guarantee the transfer of the tracked PV maximum power to the utility, the reference grid current amplitude can be calculated from the PV array power and grid voltage as follows;

$$\widehat{I_{gref}}(uncompensated) = \sqrt{2}\left(\frac{P_{PV}}{V_g}\right) \tag{15}$$

where $P_{PV}$ is maximum power extracted from PV source and $V_g$ is the rms value of grid voltage. However, system losses must be taken into account to guarantee power balance at the inverter DC-link. Due to the absence of DC-link voltage loop in the proposed technique, there must be an alternative way to compensate for these losses. Thus the reference grid-current amplitude must be readjusted to;

$$\widehat{I_{gref}}(compensated) = \sqrt{2}\left(\frac{P_{PV}}{V_g} - I_{comp}\right) \tag{16}$$

where $I_{comp}$ is the rms value of the compensating current ($i_{comp}$) shown in Fig. 2. This current represents the decrease in grid current amplitude, and in turn the decrease in grid active power to compensate for system losses. Thus, power balance and flow are ensured, achieving DC-link voltage stabilize by nature.

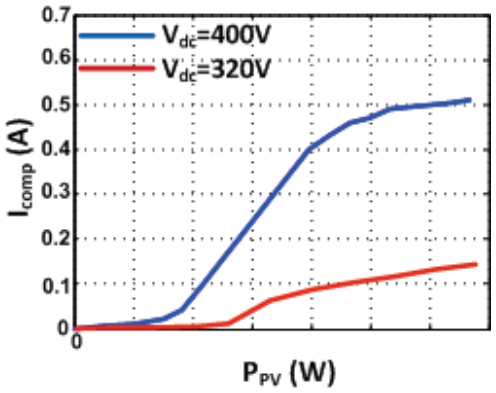


Fig. 5. Mapping between $P_{PV}$ and $I_{comp}$

At certain $V_{dc}$, as $P_{PV}$ increases system losses increase which requires the increase of $I_{comp}$ to compensate for these losses. Hence, for constant $V_{dc}$, $I_{comp}$ depends on $P_{PV}$ and changes proportionally with it however in a non-linear form. Moreover, as $V_{dc}$ increases, for constant $P_{PV}$, energy acquired by the DC-link capacitor increases which results in an increase in $I_{comp}$ to compensate for this energy. Figure 5 shows the non-linear relation between $P_{PV}$ and $I_{comp}$ for two different $V_{dc}$ values. It can be noticed that at $V_{dc}$=320V (i.e. $m_a$≈1), $I_{comp}$ has lower value which in turn decreases utility losses.

Hence, mapping between $P_{PV}$ and $I_{comp}$, at a predetermined $V_{dc}$ level, is system-dependent and mandatory in order to achieve the proposed DC-link voltage sensor-less scheme. The $P_{PV}$-$I_{comp}$ mapping can be implemented using a simple look-up table. However, for more precise mapping and better system performance, a simple feed-forward back-propagation neural network (NN) is created and utilized in the proposed technique [25]. It consists of an input layer, one hidden layer and an output layer as shown in Fig. 6. The input represents the PV power while the output layer gives the compensating current which corresponds to the input PV power and is required to stabilize $V_{dc}$ at a predetermined level. The applied hidden layer features 10 sigmoid neurons. Successful fitting between $P_{PV}$ and $I_{comp}$ depends on the hidden layer and how well the NN is trained to optimize the weights of links between nodes. The utilized NN is off-line trained where the number of the applied training epochs is ten to give almost zero mean square error for the studied case.

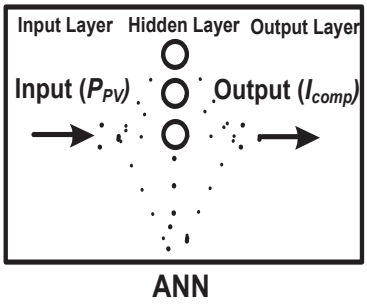


Fig. 6. Appllied neural network configurtion

## V. SIMULATION RESULTS

The transient and steady-state performance of the conventional scheme is compared to that of the proposed, under two step changes in irradiance; from 1000 W/m$^2$ to 600 W/m$^2$ at 0.6 sec then from 600 W/m$^2$ to 800 W/m$^2$ at 0.9 sec. The DC-link voltage is adjusted at 320V to decrease utility power losses as described in the previous subsection.

As shown in Fig. 7, both techniques succeed in extracting PV maximum power for different irradiance levels. Fig. 8 shows that the DC-link voltage, for both schemes, stabilizes at 320V. Finally, Fig. 9 shows the grid current acquired by both techniques during irradiance changes. Simulation results are analyzed and performance parameters are given in Table I.

At system start-up (Fig. 8.a and Table I), $V_{dc}$ overshoot in the conventional technique is larger than that of the proposed one by about 80 V, thus $C_{dc}$ of the former must handle this voltage increase. On the other hand, $V_{dc}$ adjustment takes much more time, in the proposed scheme, which increases transient power losses. However, once the required $V_{dc}$ level is reached, the proposed scheme shows better transient response for sudden irradiance changes, due to the elimination of outer loop controller. This is shown as follows;

During the first irradiance step change at t=6sec, radiation decreases, thus $P_{pv}$ will decrease causing a transient decrease in $V_{dc}$ till it is regulated to 320V. Analyzing Fig. 8.b, 9.b and Table I, the conventional control scheme shows slower response by about 0.3 sec. Furthermore, it experiences $V_{dc}$ which transiently decreases to 300V i.e. $m_a$ >1. Thus, the grid current THD goes transiently beyond acceptable limits (= 31.42 %) according to IEEE Std. 519 [26]. On the other hand, the proposed technique shows faster response and transient $V_{dc}$ decrease to 310 V i.e. $m_a$≈1. Hence, its grid current THD is within limits (= 6.3%) during its transient period.

During the second irradiance step change at t= 9 sec, radiation increases, thus $P_{PV}$ increases causing transient increase in $V_{dc}$ .Considering Fig. 8.c, 9.c and Table I, the conventional scheme exhibits longer settling time and transient $V_{dc}$ increase to 360V causing transient increase in utility power loss by almost 25% of its steady-state value (80 W). However, the proposed scheme shows almost non significant $V_{dc}$ increase during its transient period.

Finally, considering the steady-state results shown in Table I, both schemes gave close results which proves the validity and feasibility of the proposed technique.

TABLE I
TRANSIENT AND STEADY-STATE PERFORMANCE PARAMETERS

| Irradiance (W/m$^2$) | Con. Tech | Transient for $V_{dc}$ | | Steady-state | | | |
|---|---|---|---|---|---|---|---|
| | | *Over/ Under Shoot* | $t_{sett.}$ (sec) | $\Delta v$ *p-p* | *Power losses* | *THD* | *Phase shift* |
| Start-1000W/m$^2$ | Conv. | + 68.75% | 0.4 | 50V | 92 W | 3% | 1$^o$ |
| | Prop. | + 43.75% | 4 | 50V | 98 W | 2% | 0$^o$ |
| From 1000 to 600W/m$^2$ | Conv. | – 6.25% | 0.4 | 30V | 74.5W | 3.8% | 0.8$^o$ |
| | Prop. | – 3.13% | 0.1 | 30V | 74.8W | 3% | 0.1$^o$ |
| From 600 to 800W/m$^2$ | Conv. | + 12.5 % | 0.2 | 40V | 80W | 3.2% | 1$^o$ |
| | Prop. | +1.5% | 0.07 | 40V | 80.5W | 2.2% | 0$^o$ |

## VI. CONCLUSION

This paper proposes a novel DC-link voltage sensorless control technique, for single-phase two-stage PV-grid connected systems, which eliminates the DC-link voltage control loop. Alternatively, a new adjustment method of reference grid current is presented to transfer the PV power to the utility. Thus, energy balance is achieved at the DC-link and DC voltage stabilizes at a predetermined level. Consequently, control scheme complexity is minimized and system stability is enhanced. Moreover, high DC-link voltage sensor elimination reduces the system size and cost. Simulation results are analyzed to evaluate proposed technique performance and compare it with that of the conventional one. Although the novel technique is slower to stabilize the DC-link voltage at start-up, once the required DC-link voltage is reached, the proposed technique shows better transient response during sudden irradiance changes. At steady-state, both techniques give close results, which validates the proposed technique effectiveness.

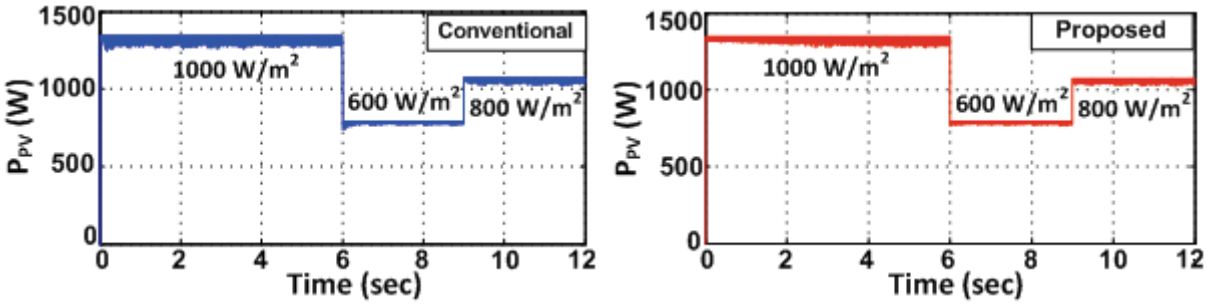


Fig. 7. Maximum power extracted from PV string using conventional and proposed techniques at three different irradiance levels

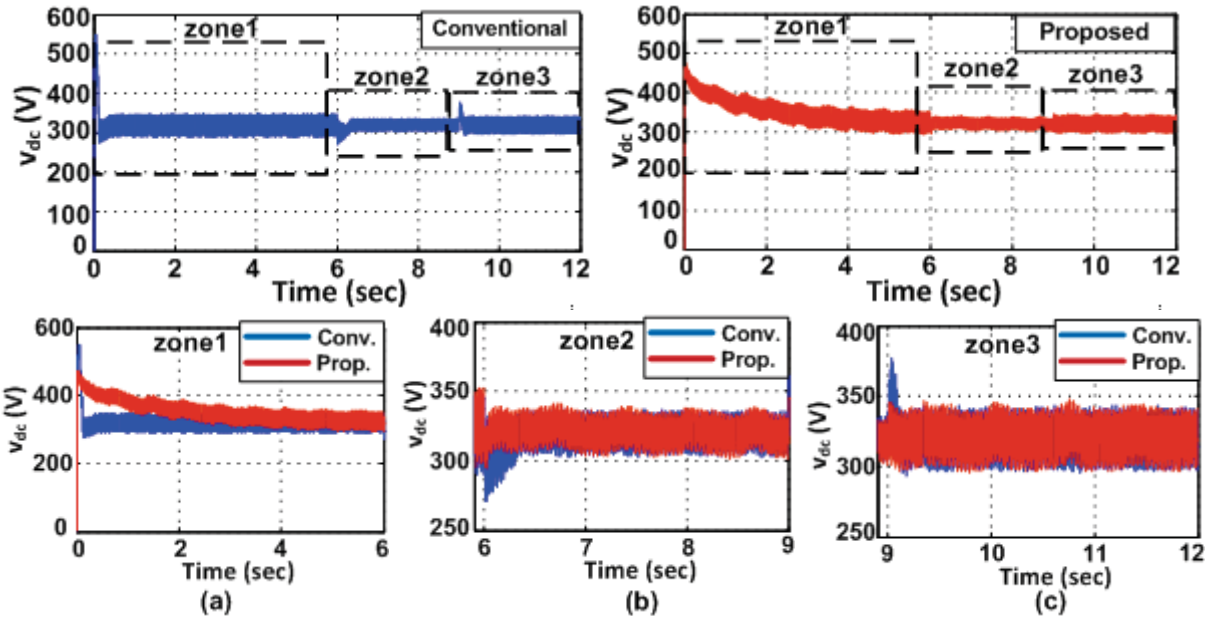


Fig. 8. DC-link voltage for conventional and proposed techniques at variable irradiance levels; (a)1000 W/m$^2$, (b) 600 W/m$^2$, (c) 800 W/m$^2$

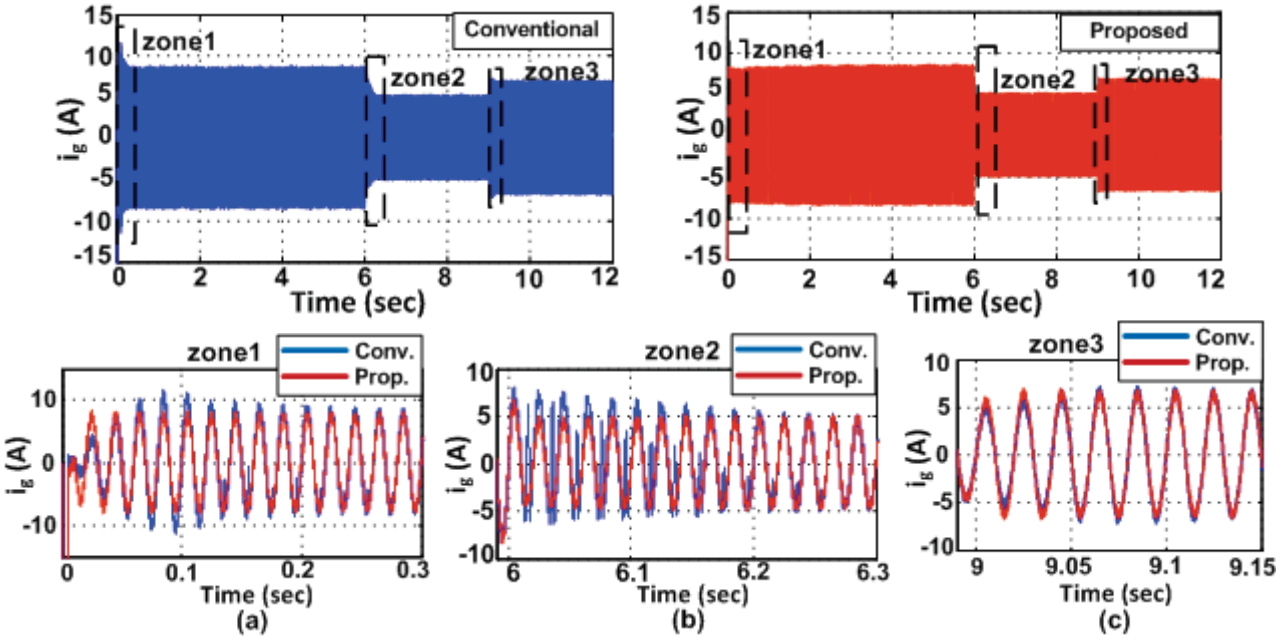


Fig. 9. Grid current for conventional and proposed techniques during; (a) Start-up, (b) First step change, (c) Second step change

## REFERENCES


[1] M. Liserre, T. Sauter, and J. Y. Hung, "Future energy systems: Integrating renewable energy sources into the smart power grid through industrial electronics", *IEEE Industrial Electronics Magazine*, vol. 4, no.1, pp.18-37, March 2010.

[2] S. V. Araújo, P. Zacharias, and R. Mallwitz, "Highly efficient single-phase transformerless inverters for grid-connected photovoltaic systems ", *IEEE Trans. Industrial Electronics*, vol. 57, no. 9, pp. 3118-3128, Sep. 2010

[3] S. B. Kjaer, J. K. Pedersen, and F. Blaabjerg," A review of single-phase grid-connected inverters for photovoltaic modules", *IEEE Trans. Industry Applications,* vol. 41, no. 5, pp.1292-1306, Sep/Oct 2005

[4] J. Myrzik and M. Calais, "String and module integrated inverters for single-phase grid connected photovoltaic systems - a review," in *Proc. IEEE Power Tech Conf.*, vol. 2, June 2003.

[5] S. Chowdhury, S.P. Chowdhury and P. Crossley, *Microgrids and Active Distribution Networks*, IET Renewable Energy Series 6, Institution of Engineering and Technology, London, 2009

[6] F. Blaabjerg, R. Teodorescu, M. Liserre, and A. V. Timbus, " Overview of control and grid synchronization for distributed power generation systems", *IEEE Trans. Industrial Electronics*, vol. 53, no. 5, pp. 1398-1409, October 2006.

[7] M. A. Eltawil, and Z. Zhao, " Grid-connected photovoltaic power systems: Technical and potential problems—A review", *ELSEVIER Trans. Renewable and Sustainable Energy Reviews*, vol. 14, no. 1, pp. 112–129, January 2010.

[8] S. Jain and V. Agarwal, "A single-stage grid connected inverter topology for solar PV systems with maximum power point tracking," *IEEE Trans. Power Electronics*, vol. 22, pp. 1928–1940, Sept. 2007.

[9] S. Jain, and V. Agarwal, "Comparison of the performance of maximum power point tracking schemes applied to single-stage grid-connected photovoltaic systems," *IET Electric Power Applications,* vol. 1, no. 5, pp. 753-762, Sept. 2007.

[10] Y. M. Chen, C. H. Chang, H. C. Wu, "DC-Link capacitor selections for the single-phase grid-connected PV system", *in Proc. International Power Electronics and Drive Systems Conf.(PEDS'09),* 2009, pp.72 – 77

[11] T. Shimizu, K. Wada, and N. Nakamura, "Flyback-type single-phase utility interactive inverter with power pulsation decoupling on the dc input for an ac photovoltaic module system," *IEEE Trans. Power Electronics*, vol. 21, no. 5, pp. 1264–1272, Sept 2006.

[12] N. A. Ninad and L. A. C. Lopes, "Operation of single-phase grid-connected inverters with large DC bus voltage ripple", *in Proc. IEEE Electrical Power Conf.* (EPC '07), 2007, pp. 172-176.

[13] R. J. Wai and W. H. Wang, "Grid-connected photovoltaic generation system," *IEEE Trans. Circuits and Systems*, vol. 55, no. 3, pp 953- 964, .April 2008.

[14] N. Femia, G. Petrone, G. Spagnuolo, and M. Vitelli, "A technique for improving P&O MPPT performances of double-stage grid-connected photovoltaic systems," *IEEE Trans. Industrial Electronics*, vol. 56, no. 11, pp. 4473-4482, Nov. 2009

[15] C. Meza, D. Biel, J. Negroni, and F. Guinjoan, "Boost-buck inverter variable structure control for grid-connected photovoltaic systems with sensorless MPPT" *in Proc. IEEE Inter.Symposium on Industrial Electronics (ISIE '05),* vol. 2, 2005, pp. 657 – 662.

[16] N. A. Rahim, J. Selvaraj, Krismadinata, "Hysteresis current control and sensorless MPPT for grid-connected photovoltaic systems", *in Proc Inter. Symposium on Industrial Electronics (ISIE),*2007, pp. 572-577

[17] B. Yang, W. Li, Y. Zhao, and X. He, "Design and analysis of a grid-connected photovoltaic power system," *IEEE Trans. Power Electronics*, vol. 25, no. 4, pp. 992-1000, April 2010.

[18] Y. Kim ; J. Kang ; S. Youn ; Y. Jung ; C. Won, "Sensorless current balancing and MPPT control for photovoltaic AC module type interleaved flyback inverter ", *in Proc. Power Electronics and Motion Control Conf. (IPEMC)*, vol. 2, pp. 1363 – 1367, June 2012

[19] T. Kitano, M. Matsui, D. Xu, "A maximum power point tracking control scheme for PV system based on power equilibrium and its system design", *IEEJ Trans. Industry App.*, vol.121, no.12, 2001, pp.1263-1269.

[20] T. Kitano, M. Matsui, D. Xu, "Power sensor-less MPPT control scheme utilizing power balance at DC link –system design to ensure stability and response," *in Proc. IEEE Industrial Electronics Society Conf., ( IECON'01)*, 2001, pp. 1309-1314.

[21] D.W. Hart, *Power Electronics Handbook*. McGraw Hill, New York, 2011.

[22] B. Farhangi, S. Farhangi, "Comparison of z-source and boost-buck inverter topologies as a single phase transformer-less photovoltaic grid-connected power conditioner", *in Proc. IEEE Power Electronics Specialists Conf. (PESC '06)* , 2006 , pp. 1 - 6

[23] A. Kotsopoulos, J. L. Duarte, and M. A. M. Hendrix, "Predictive DC voltage control of single-phase PV inverters with small DC link capacitance", *in Proc. IEEE International Symposium on Industrial Electronics (ISIE '03),* vol. 2, 2003, pp. 793 – 797.

[24] F. Liu, S. Duan, F. Liu, B. Liu, and Y. Kang, "A variable step size INC MPPT method for PV systems", *IEEE Trans. Industrial Electronics,* vol. 55, no. 7, pp. 2622-2628, July 2008.

[25] M.T. Hagan, H.B. Demuth, and M.H. Beale, *Neural Network Design*, MA: PWS Publishing, Boston, 1996.

[26] IEEE, "IEEE Recommended Practices and Requirements for Harmonic Control in Electric Power Systems," *IEEE Std. 519-1992*.